CHARACTERIZATION OF PRECIPITATION-STRENGTHENING HEAT-RESISTANT AUSTENITIC STAINLESS STEELS FOR LIFE-PREDICTION MODELING

Yukinori Yamamoto, Qing-Qiang Ren, Rishi Pillai, David Hoelzer, Michael Brady, Yajie Zhao, Jonathan Poplawsky, Edgar Lala-Curzio
Oak Ridge National Laboratory, Oak Ridge, Tennessee, USA

Arul Kumar Mariyappan, Ricardo Lebensohn, Laurent Capolungo
Los Alamos National Laboratory, Los Alamos, New Mexico, USA

Michael Glazoff
Idaho National Laboratory, Idaho Falls, Idaho, USA

Michael Gao, Martin Detrois, Paul Jablonski, Jeffery Hawk*, David Alman
*National Energy Technology Laboratory, Albany, OR, USA (*retired)*

ABSTRACT

In this study, the role of minor alloying additions in 347H stainless steels (UNS34709, ASTM A240/240M) on creep-rupture properties at 650-750°C and microstructure evolution during isothermal exposure at 750°C has been investigated, aiming to provide the experimental dataset as boundary conditions of physics-based modeling for material/component life prediction. Four different 347H heats containing various amounts of boron and nitrogen additions were prepared and evaluated. The combined additions of B and N are found to stabilize the strengthening secondary $M_{23}C_6$ carbides and retarding the transition from $M_{23}C_6$ to sigma phase precipitates during thermal exposure. The observed kinetics of microstructure evolution reasonably explains the improvement of creep-rupture properties of 347H stainless steels with the B and N additions.

INTRODUCTION

A multi-national laboratory project to establish the accelerated methods for designing and developing high-temperature structural alloys for extreme environments is currently underway, so-called "eXtremeMAT (XMAT)", under Crosscutting Technology High Performance Materials Research Program, Office of Fossil Energy and Carbon Management, U.S. DOE [1]. The project framework consists of a computational approach to describe and predict material deformation of selected model alloys at elevated temperatures which incorporates the dynamic plasticity model [2,3], density functional theory, thermodynamics, and the predicted kinetics of the strengthening secondary precipitation [4,5], together with experimental validation [6-9], to be used for newly proposed physic-based material/component life assessment modeling.

The project selected 347H stainless steel (UNS34709 under ASTM A240/240M) as one of the model high-temperature structural alloys consisting of "FCC matrix" with "precipitation strengthening", to systematically analyze and predict the material responses under potential service conditions. Although the steel is commercially available and its properties and microstructure have been widely investigated [10-14], the project newly prepared multiple 347H heats with known pedigrees to evaluate the relationship among the chemistry, process and thermal history, mechanical properties, and microstructure. One key element of this project involves the fabrication of model 347H stainless steels with and without additions of nitrogen and boron, evaluating the material responses after isothermal aging and uniaxial creep tests as a function of temperature, stress, and alloy composition, and then correlating the results with microstructure through multi-scale characterization. In this study, the role of minor alloying additions in 347H stainless steels on creep-rupture properties and microstructure evolution during isothermal exposure has been evaluated. The amounts of the strengthening/deteriorating secondary phase precipitates are quantitatively analyzed and correlated with the creep-rupture behavior, aiming to provide the property/microstructural dataset as boundary conditions of physics-based modeling under XMAT project.

EXPERIMENTAL PROCEDURES

Four different 347H stainless steel heats were prepared through a vacuum induction melting at the Melt Processing Laboratory of National Energy Technology Laboratory. These alloys were cast into columnar-shape ingots with ~30kg targeting the composition met with a standard of 347H stainless steel (UNS34709, ASTM A240/240M) with various amounts of the N and B additions. 347H-hp (high purity) followed the compositional specification with the elements described in the standard (Fe, Cr, Mn, Ni, Si, Nb, and C), and 347H-N and 347H-NB intentionally added N and B within the ranges observed in commercial 347H stainless steels [14]. 347H-NB+ containing almost doubled amounts of N and B compared to those in 347H-NB. The ingots were thermo-mechanically treated, including homogenization, hot-forging, and hot-rolling, to make plate samples with a thickness of ~10 mm. The rolled plates were annealed at 1100°C, followed by water quenching, which achieved a fully recrystallized, solution-annealed microstructure with a small amount of residual primary NbC dispersed in the FCC-Fe (austenite) matrix. Table 1 summarizes the analyzed compositions of the 347H heats, measured through inductively coupled plasma atomic emission spectroscopy for major elements, combustion-infrared absorbance for C, inert gas fusion for N, and inductively coupled plasma mass spectroscopy for B.

Table 1. Analyzed compositions of 347H stainless steel heats studied.

Alloy ID	Analyzed composition, wt.%								wppm			
	Fe	Cr	Mn	Ni	Al	Si	Nb	C	B	N	O	S
347H-hp	68.43	18.52	0.98	11.03	<0.01	0.39	0.50	0.0508	5	22	52	23
347H-N	68.69	18.37	0.93	10.97	0.01	0.42	0.51	0.0531	<5	163	80	<10
347H-NB	68.49	18.38	0.92	10.97	<0.01	0.46	0.57	0.0553	11	168	54	10
347H-NB+	68.74	18.35	0.96	10.94	<0.01	0.39	0.50	0.0526	32	323	162	33

Tensile creep specimens with a round-shape gage section with 6.4 mm in diameter and 31.8mm in length and threaded grips were machined from the annealed 347H plates, with the tensile axis parallel to the rolling direction. Creep-rupture tests were conducted at 650 and 750°C in laboratory air with a constant loading condition in a range from 35 to 265 MPa. The creep-deformation was measured by a couple of linear variable differential transformer attached to the specimen via an extensometer. Isothermal aging at 750°C in laboratory air was conducted for

various periods of time up to 10,000h. Small pieces sectioned from the annealed 347H plates were aged in a tube furnace with the temperature control within ± 2°C, and then water-quenched after aging. Microstructure characterization was conducted by optical and scanning electron microscopies (OM and SEM, respectively), and most of the SEM images were acquired through back-scattered electron (BSE) mode. The rolling direction or tensile axis are always parallel to the horizontal axis in each image in the present study. Crystallographic orientation distribution was measured by electron back-scattered diffraction (EBSD) technique, and phase identification of the primary/secondary phase precipitates was made by compositional analysis through energy dispersive x-ray spectroscopy (EDS). The volume fractions of the secondary phase precipitates were measured through an image analysis software using manually colored, binarized SEM-BSE images.

RESULTS AND DISCUSSION

Initial microstructure

The as-processed microstructure of all 347H heats consisted of uniform, equiaxed austenite grains with an average grain size of ~ 50μm and primary NbC particles with a size of ~1 μm dispersed in the austenite matrix. Figure 1 represents SEM characterization results; a SEM-BSE image showing typical microstructure of 347H-hp (1a) and a IPF color map acquired through SEM-EBSD showing crystallographic orientation at each grain perpendicular to the image (1b). Primary NbC particles were uniformly distributed in the entire plate sample, and no specific texture was observed in the microstructure. Microstructure characteristics of the other 347H heats were almost identical to those of 347H-hp.

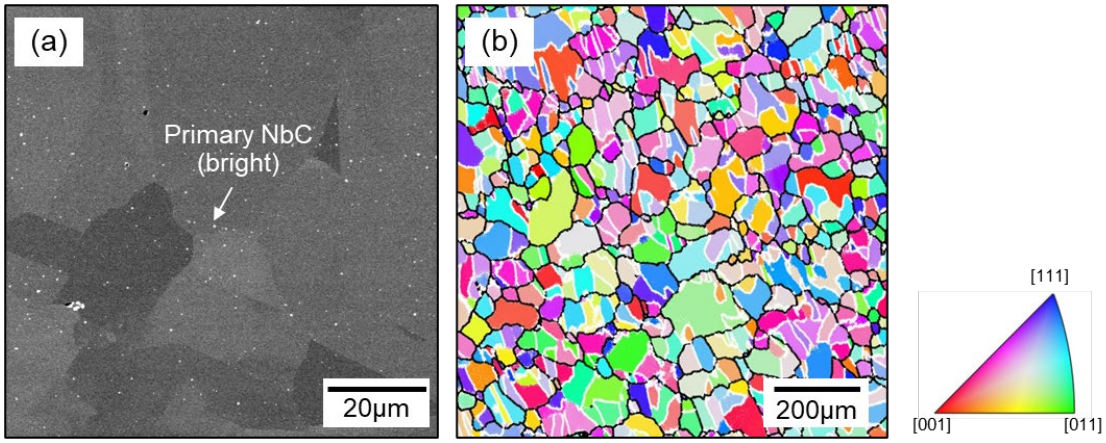

Figure 1. The initial microstructure of 347H-hp: (a) SEM-BSE image and (b) IPF color map showing crystallographic orientation of grains perpendicular to the image. The black and white lines represent general and twin boundaries, respectively.

Creep-rupture properties

Figure 2 compares the creep-rupture curves of 347H-hp, 347H-NB, and 347H-NB+ tested at 750°C. In overall test results, 347H-hp showed less creep-deformation resistance than the others at a given test condition, including shorter creep-rupture life and higher minimum creep-rate. The tests at 60 or 65MPa resulted in relatively short-term tests with less than 3,000h of creep-rupture lives (2a). It demonstrated a lower creep resistance in 347H-hp (rupture life: 1,162h) than those in 347H-NB and 347H-NB+ (2,069 and 2,262h, respectively), even with a slightly higher stress condition in the latter, suggesting the positive effect of the N and B additions on creep-rupture

properties in 347H stainless steels. The same trend was observed in the tests with 50MPa which achieved ~10,000h creep-rupture lives in 347H-NB/-NB+, while 347H-hp ruptured only after 2,262h at the same test condition. It should be emphasized that 347H-NB showed longer creep-life than 347H-NB+ at 65MPa testing despite higher additions of N and B in the latter, whereas the tests at 50MPa led to an opposite result with longer creep-life in 347H-NB+.

The effect of B on creep-rupture properties in 347H stainless steels was reported by Abe [14], which indicated that creep-rupture life of 347H stainless steels at 700°C increased with the B addition linearly up to 15 wppm. This is consistent with the present results in 347H-hp. However, the report by Abe [14] also mentioned that no significant change was observed between 15 to 27 wppm of B, which did not match with the observed results in 347H-NB and 347H-NB+.

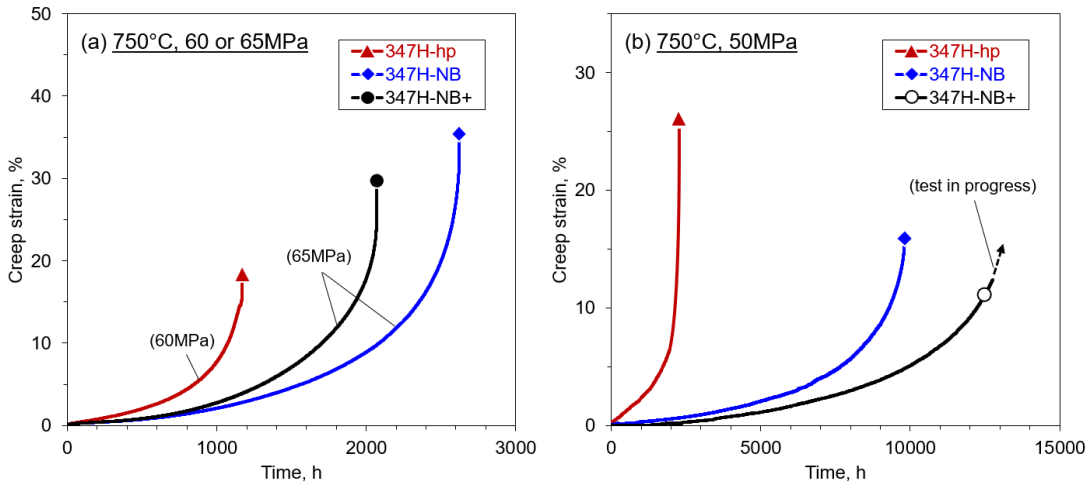

Figure 2. Comparison of creep-rupture curves among three different 347H stainless steels tested at 750°C: (a) 60 or 65MPa, and (b) 50MPa.

All creep-rupture test results tested at 650 and 750°C are summarized in Figure 3, showing the creep-rupture lives (3a) and the minimum creep-rate (3b) plotted as a function of stress. Tests at 750°C captured the trends described above: 347H-NB showed longer creep-rupture lives and lower minimum creep-rates than those of 347H-NB+ in relatively short-term creep regime, whereas they started being opposite in long-term creep regime. The transition appeared at a creep-rupture life around 3,000h or a stress between 50 and 65 MPa. At 650°C, on the other hand, these two heats did not show apparent discrepancies in both creep-lives and minimum creep-rates in the stress conditions studied. 347H-hp always showed ~20-25% lower creep strength than the others in the range of this study at both 650 and 750°C.

As discussed later, the observed creep-rupture behaviors are considered being strongly correlated with the kinetics of the strengthening/deteriorating secondary phase precipitation. It should be emphasized that the stress exponents, n, obtained from the minimum creep rates shown in Figure 3b ranged from 4.4 to 7.0, suggesting that the dislocation creep was considered as a dominant mechanism for all creep deformation. In other words, precipitation strengthening was dominantly controlling the material deformation in the ranges of the present study. Therefore, the obtained stress components indirectly explained that the variation of creep-rupture behaviors among three different 347H heats was attributed to the precipitation behavior of the secondary phase during creep testing.

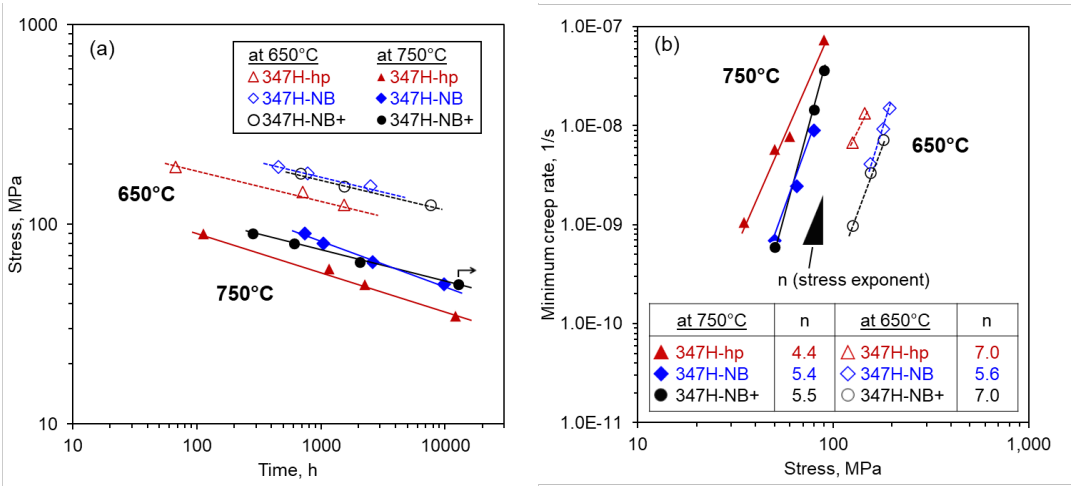

Figure 3. Creep-rupture test results of three different 347H stainless steels tested at 650 and 750°C: (a) creep-rupture lives and (b) minimum creep-rates plotted as a function of stress.

Figure 4 shows the SEM-BSE images of 347H-hp and 347H-NB after creep-rupture testing at 750°C, comparing the microstructures at the gage with similar creep-rupture lives in both materials within short- (4a and 4c) and long-term (4b and 4d) creep regimes. In 347H-hp, sigma phase precipitates (bright-contrast particles in the image) were observed on the grain boundaries after testing for 2,262h, and the amount of sigma phase increased in the specimen tested for 12,136h. On the other hand, 347H-NB showed no sigma phase precipitates after testing for 2,622h, whereas sigma phase appeared in the specimen tested for 9,813h. Sigma phase formation leads to deterioration of creep performance in 347H steels, since the strengthening, meta-stable $M_{23}C_6$ carbides (M: mainly Cr) formed in the early stage of creep testing disappears during prolonged thermal exposure by the formation of stable sigma phase [6,13,15]. Therefore, the microstructure characterization results are in a good agreement with the variation of creep-rupture properties between 347H-hp and 347H-NB: the addition of N and B significantly delays the transition from $M_{23}C_6$ to sigma phase delays, which leads to a delay of tertiary creep and increases the creep-rupture life at a given stress condition. A DFT analysis reported by Yu *et al.* [5] revealed that the B addition increased the phase stability of meta-stable $M_{23}C_6$ in FCC-Fe, which also supported the observed precipitation kinetics.

Isothermal aging

The authors previously reported that 347H-hp formed meta-stable $M_{23}C_6$ carbides in the early stage of isothermal aging at 750°C, and the carbides transformed to sigma phase after 336h aging [6]. To quantitatively analyze the effect of the N and B additions on microstructural stability, microstructure characterization of four different 347H heats (347H-hp and 347H-N/-NB/-NB+) was conducted after isothermal aging at 750°C, especially focusing on $M_{23}C_6$ and sigma phase. Figure 5 shows SEM-BSE images of 347H-hp [6] and 347H-NB+ after isothermal aging. In 347H-hp, almost no $M_{23}C_6$ carbides but only sigma phase precipitates were observed after aging for 3,000h (5a), and the amount of sigma phase increased after aging for 10,000h (5b). The amounts and distribution of sigma phase precipitates showed no significant difference from the microstructure after creep-rupture testing shown in Figure 4, suggesting that the creep-deformation would not strongly impact on the precipitation kinetics of sigma phase. On the other hand, in 347H-NB+, $M_{23}C_6$ carbides were observed on grain boundary after 168h aging, and the size were almost unchanged during aging up to 10,000h (5c and 5d). A small amount of sigma phase precipitates was observed only in the specimen after aging for 10,000h.

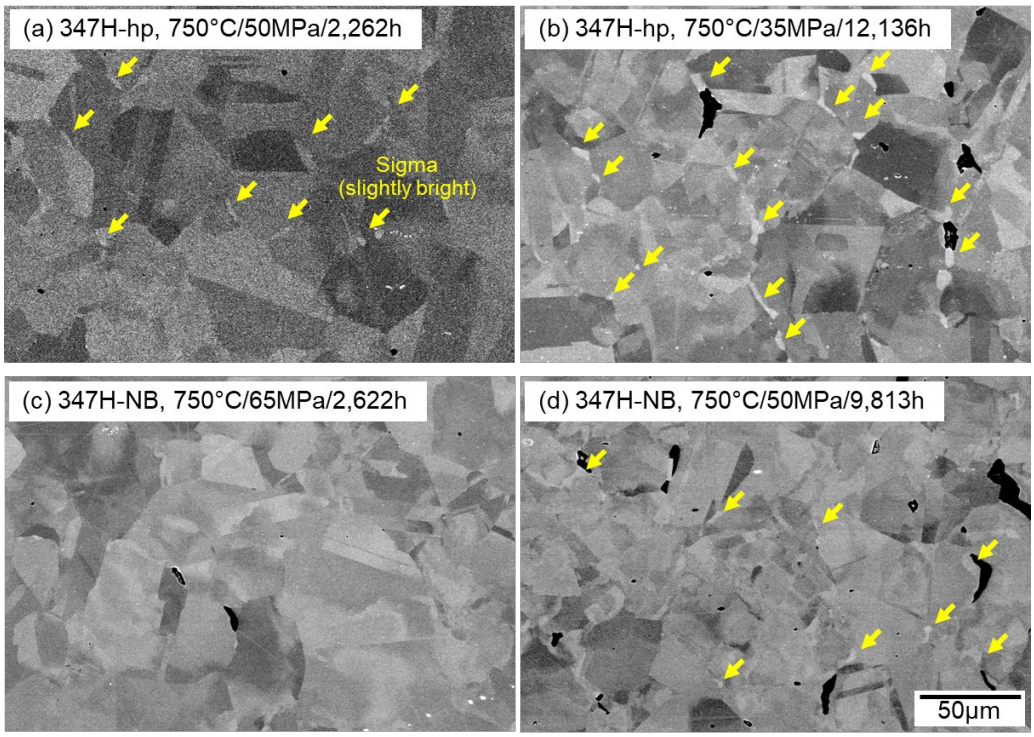

Figure 4. SEM-BSE images of 347H-hp (a and b) and 347H-NB (c and d) after creep-rupture testing at 750°C: (a) 50 MPa, (b) 35MPa, (c) 65MPa, and (d) 50MPa. The dark contrast regions in the images correspond to the creep-voids, and the yellow arrows indicate sigma phase precipitates.

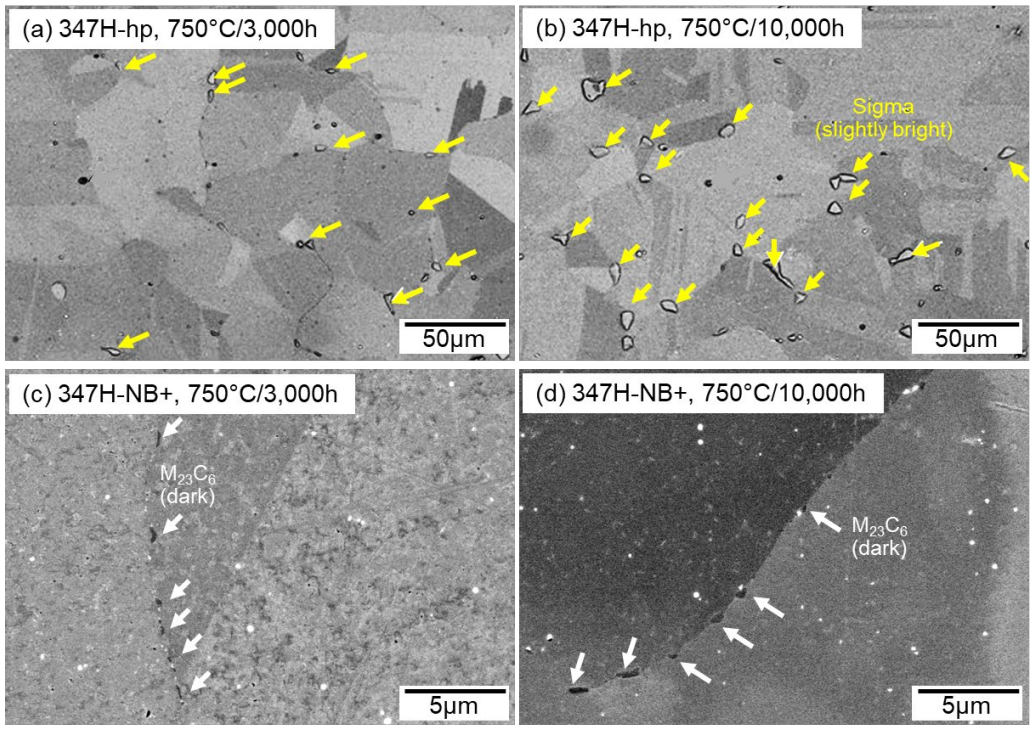

Figure 5. SEM-BSE images of 347H-hp (a and b [after ref. 6]) and 347H-NB+ (c and d) after isothermally aging at 750°C for (a) 3,000h, (b) 10,000h, (c) 3,000h, and (d) 10,000h. The yellow and white arrows indicate sigma phase precipitates and $M_{23}C_6$ carbides, respectively.

The measured volume fractions of $M_{23}C_6$ carbides and sigma phase precipitates in 4 different 347H heats are compared after isothermal aging at 750°C for 1,000h, 3,000h, and 10,000h, as shown in Figure 6. All 347H heats form $M_{23}C_6$ carbides first, mainly on grain boundaries, and then they turned to sigma phase precipitates as replacement of $M_{23}C_6$. In 347H-hp, no $M_{23}C_6$ but only sigma phase was observed after 336h aging [6], as mentioned earlier. The amount of sigma phase increased monotonically up to 10,000h. The addition of 163 wppm N in 347H-N resulted in a delay of the transition from $M_{23}C_6$ to sigma phase compared to 347H-hp, resulting in less amount of sigma phase formation than that of 347H-hp at a given aging time. 347H-NB showed relatively large amount of $M_{23}C_6$ after aging for 1,000h and 3,000h, and then the amount significantly reduced after 10,000h. Instead, sigma formed after 3,000h and then increased as opposed to the reduction of $M_{23}C_6$. 347H-NB+ formed $M_{23}C_6$ with the amount continuously increasing with aging up to 10,00h, and the volume fraction exceed that in 347H-NB after 10,000h. Sigma phase was observed only after 10,000h in 347H-NB+. By comparing 347H-NB (168 wppm N) and 347H-NB+ (323 wppm N), it is considered that the increased N addition also causes a delay of the transition from $M_{23}C_6$ to sigma, as observed in the comparison between 347H-hp and 347H-N.

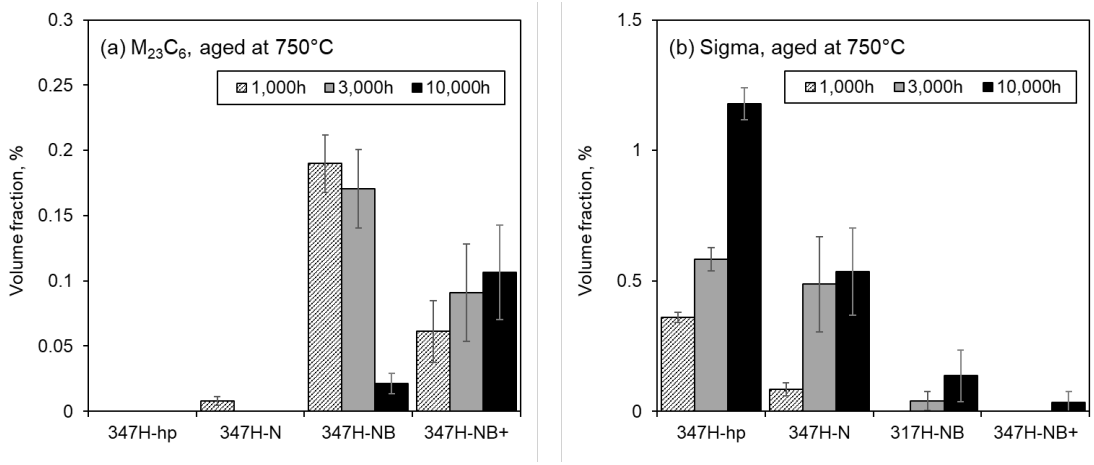

Figure 6. Volume fractions of M23C6 carbides (a) and sigma phase precipitates (b) observed in four different 347H stainless steels after isothermal aging at 750°C.

Based on the secondary phase precipitation kinetics described above, it is hypothesized that the gaps in the creep-rupture properties between 347H-NB and 347H-NB+ at 750°C are strongly correlated with the changes in the secondary phase precipitates. In the short-term creep regime (below 3,000h creep-lives), larger amounts of $M_{23}C_6$ carbides in 347H-NB contribute to longer creep-rupture life and lower minimum creep rate than those in 347H-NB+. In the long-term creep regime, the delay of sigma phase formation in 347H-NB+ impacts positively to extend the creep-rupture life compared to 347H-NB at a given stress condition. Although no detailed characterization was conducted in the creep-rupture specimens tested at 650°C, the formation of sigma phase at 650°C may require significantly longer thermal exposure than that at 750°C due to slower diffusion [13]. Therefore, no apparent discrepancy in microstructure evolution is expected between 347H-NB and 347H-NB+ at 650°C, at least in the range of test duration in this study, which leads to the observed the creep-rupture test results at 650°C in these two 347H heats.

This study experimentally demonstrated that the additions of B and N strongly impacted on kinetics of the secondary phase precipitation, $M_{23}C_6$ and sigma, and caused the variation of creep-rupture properties among the 347H heats. The B addition significantly improves the stability of $M_{23}C_6$ in FCC-Fe matrix, and the N addition slower the transition from $M_{23}C_6$ to sigma during thermal exposure, resulting in increasing the creep-rupture life of 347H steels as observed. However, the mechanism how the N addition changes the precipitation kinetics is still unclear

from the present study. The effect of secondary MX (M = Nb, X = C and N) carbides/ carbonitrides on precipitation strengthening has not been discussed either. Further detailed characterization is currently in progress to investigate the undiscussed items.

SUMMARY

In this study, the effect of the B and N additions in 347H stainless steels on creep-rupture properties at 650-750°C and microstructure evolution during isothermal exposure at 750°C were evaluated. Four different 347H heats with and without various amounts of the boron and nitrogen additions were prepared under the present study to evaluate the materials with known pedigrees. The combined additions of B and N in 347H stainless steels improve the creep-rupture properties significantly compared to those of 347H without intentional additions of B and N. The B addition stabilizes the strengthening secondary $M_{23}C_6$ carbides, and the combined additions of B and N retards the transition from $M_{23}C_6$ to sigma phase precipitates during creep-rupture testing, which are in a good agreement with the microstructure characterization of isothermally aged 347H heats. The observed kinetics of microstructure evolution reasonably explains the improvement of creep-rupture properties of 347H stainless steels with the B and N additions. However, the present study has not fully explained the mechanism how the N addition changes the precipitation kinetics, and the role of secondary MX (M = Nb, X = C and N) on the properties has not been discussed either. Further characterization is currently in progress.

ACKNOWLEDGEMENTS

This work was performed in support of the US DOE Office of Fossil Energy and Carbon Management through the eXtremeMAT (XMAT) program under Crosscutting Technology High Performance Materials Research Program. SEM characterization was supported by the Center for Nanophase Materials Sciences (CNMS), which is a US Department of Energy, Office of Science User Facility at Oak Ridge National Laboratory.

REFERENCES

[1] DOE, U. S. *eXtremeMAT (website)*, <https://edx.netl.doe.gov/extrememat/> (2024).
[2] Kumar, M. A. & Capolungo, L., "Microstructure-sensitive modeling of high temperature creep in grade-91 alloy," *Int J Plasticity,* Vol. 158, (2022), p. 103411.
[3] Bieberdorf, N. *et al.*, "A mechanistic model for creep lifetime of ferritic steels: Application to Grade 91," *Int J Plasticity,* Vol. 147, (2021), p. 103086.
[4] Glazoff, M. V. *et al.*, "Concurrent Precipitation of Nb(C, N) and Metastable MC in Alloy 347H at 700°C and 750°C: Computer Simulations and Comparison to Experiment," *JOM,* Vol. 74, (2022), pp. 1444-1452.
[5] Yu, J. G. *et al.*, "Boron substitution induced FCC Fe/CrC interfacial strengthening: An *ab-initio* study," *Comp Mater Sci,* Vol. 228, (2023), p. 112370.
[6] Ren, Q. Q. *et al.*, "Sigma phase evolution and nucleation mechanisms revealed by atom probe tomography in a 347H stainless steel," *Materialia,* Vol. 24 (2022), p. 101485.
[7] Yamamoto, Y. *et al.*, "Creep Behavior and Phase Equilibria in Model Precipitate Strengthened Alumina-Forming Austenitic Alloys," *JOM,* Vol. 74, (2022), pp.1453-1468.
[8] Yamamoto, Y. *et al.*, "Role of Cr Content in Microstructure, Creep, and Oxidation Resistance of Alumina-Forming Austenitic Alloys at 850-900 °C," *Metals*, (2022), p. 12050717.

[9] Pillai, R. *et al.*, "Challenges in computationally designing high temperature Fe-based austenitic alloys: Addressing the role of Ni additions," *Materialia,* Vol. 28, (2023), p. 101772.
[10] Sourmail, T., "Precipitation in creep resistant austenitic stainless steels," *Materials Science and Technology,* Vol. 17, (2001), pp.1-14.
[11] Erneman, J. *et al.*, "The evolution of primary and secondary niobium carbonitrides in AISI 347 stainless steel during manufacturing and long-term ageing," *Acta Materialia.* Vol. 54, (2006), pp. 67-76.
[12] Schwind, M. *et al.*, "σ-phase precipitation in stabilized austenitic stainless steels," *Acta Materialia,* Vol. 48, (2000), pp. 2473-2481.
[13] Minami, Y. *et al.*, "Microstructural Changes in Austenitic Stainless-Steels during Long-Term Aging," *Materials Science and Technology,* Vol. 2, (1986), pp. 795-806.
[14] Abe, F., "Heat-to-Heat Variation in Creep Life and Fundamental Creep Rupture Strength of 18Cr-8Ni, 18Cr-12Ni-Mo, 18Cr-10Ni-Ti, and 18Cr-12Ni-Nb Stainless Steels," *Metall Mater Trans A,* Vol. 47a, (2016), pp. 4437-4454.
[15] Vitek, J. M. & David, S. A., "The Sigma-Phase Transformation in Austenitic Stainless-Steels," *Weld J,* Vol. 65, (1986), pp. S106-S111.